Received: 16 April 2024 | Revised: 22 November 2024 | Accepted: 23 November 2024

DOI: 10.1002/dvdy.70005

RESEARCH ARTICLE

Developmental Dynamics WILEY

Active cell proliferation contributes to the enlargement of the nascent nucleus pulposus

Rose G. Long | **Changhee Lee** | **Clifford J. Tabin**

Department of Genetics, Harvard Medical School, Boston, MA, USA

Correspondence
Clifford J. Tabin, Department of Genetics, Harvard Medical School, 77 Avenue Louis Pasteur, Boston, MA 02115, USA.
Email: tabin@genetics.med.harvard.edu

Funding information
National Institute of Arthritis and Musculoskeletal and Skin Diseases, Grant/Award Number: F32AR076226

Abstract

Background: The notochord is an embryonic organ involved in forming and patterning the spinal column. The mechanism by which the notochord transforms from a continuous rod to a segmented structure excluded from the vertebrae and residing solely as the nucleus pulposus within the intervertebral disc is understudied. The current model of notochordal segmentation suggests that swelling through formation and maturation of the vertebrate cartilage squeezes the notochord cells from the vertebra.

Results: Analysis of Collagen 10, a marker for hypertrophic differentiation, as well as evaluation of changes in cell density, reveal that the expansion of the vertebral precursor cells occurs after notochord segmentation has already taken place. We find that the bulk of the nucleus pulposus is derived from accelerated proliferation within the nucleus pulposus itself. In a model of cell proliferation, the increased proliferation at the nucleus pulposus importantly contributes to expand the nucleus pulposus area.

Conclusions: Our data is consistent with the hypothesis that notochord cell proliferation contributes to the enlargement of the nucleus pulposus before the vertebra undergo hypertrophy.

KEYWORDS

intervertebral disc, morphogenesis, spine

1 | INTRODUCTION

The mature spinal column is a metameric structure consisting of alternating vertebral bodies and intervertebral discs. Each intervertebral disc has two structural domains, a ring of somite-derived fibrous tissue, the annulus fibrosus, encircling an inner, notochord-derived tissue, the nucleus pulposus. Understanding how this repeating pattern emerges requires knowledge of the embryonic tissues from which they form. The notochord is a rod-like continuous structure running down the middle of the chordate embryo. On each side, lateral to the notochord, are epithelial balls called somites partitioned from the paraxial mesoderm.[1] The ventro-medial portion of the somite, the sclerotome, gives rise to skeletal precursors, and these sclerotome cells migrate medially to surround the notochord. The somite has rostral-caudal polarity,[2] greater cell density caudally and splits transversely along the von Ebner fissure. The caudal part of each somite fuses with the rostral part of the next lower or inferior somite. Each vertebra forms by the fusion of two halves of two somites; the highly cellularized caudal region fuses with the rostral (top) part of the inferior adjacent somite.[3–5] Meanwhile, the intervertebral disc arises from the denser caudal side of the original somite. The mesenchyme giving rise to the intervertebral disc and vertebra is wrapped around the notochord by E12.5. Two days later, at E14.5, the notochord is expanding into

the intervertebral disc and shrinking in the vertebra, such that the ratio of the notochord diameter at the intervertebral disc to the notochord diameter at the vertebral body is increasing. The notochord expansion gives rise to the nucleus pulposus, the center of the intervertebral disc.[6,7] The dissolution of the notochord into the nucleus pulposus is essential for maintenance of the annulus fibrosus and formation of the spinal column,[8,9] yet the cell dynamics underlying this transformation are unclear. The cell dynamics may yield other active processes in proper segmentation; rarely, remnants of the notochord remaining in the vertebra,[10] specifically at the saccrum or at the base of the skull[11] can give rise to a devastating cancer called chordoma.[12] Chordoma can be associated with an increased copy number of the gene encoding the transcription factor brachyury,[13] but many cases do not show brachyury duplication,[14] indicating other processes may be active.

The current hypothesis for the transition of the notochord to nucleus pulposus is that as the hypertrophic chondrocytes of the vertebral bodies deposit extracellular matrix and expand, they squeeze the notochord out of the vertebral anlagen and into the intervertebral space.[7,15,16] In support of this model, in normal mice, there is evidence that chondrocyte hypertrophy, specifically proteoglycan deposition and Pax1 exclusion, starts before the notochord starts to decrease in diameter in the vertebral regions, the first sign of notochord segmentation.[17] Moreover, the notochord is not segmented in Col2al-null mice which are defective in chondrocyte differentiation.[16] Leveraging a later hypertrophy extracellular matrix protein, Collagen 10,[18] could determine what stage is necessary for notochord exclusion. Similarly, in Sox5, Sox6 double knock-out mice, in which the vertebra eventually fail to undergo hypertrophy, the notochord remains in the vertebra, not confined within the intervertebral mesenchyme.[19] It is important to note, however, that additionally, in the Sox5, Sox6 double knock-out mice, the notochord sheath, which normally surrounds the notochord from early stages, does not form, and there is widespread notochordal cell death,[17] suggesting a second role for these transcription factors in creating the notochordal sheath, in addition to controlling chondrogenesis.[20,21] In normal mice, the notochordal sheath thickens before transformation of the notochord, but attenuates during the intervertebral expansion.[22]

In spite of the evidence for a role of the vertebral expansion in notochord segmentation, there could also be contributions to the process from notochord autonomous mechanisms. The notochord persists in vertebra as a wavy continuous rod when the sclerotome fails to migrate ventrally around the notochord in NKX3-2−/− mutant.[23] In these mice, the notochord increases diameter in the forming intervertebral discs in the absence of most of the surrounding anterior sclerotomal mesenchyme in the adjacent undifferentiated vertebral bodies. This raises the possibility that the notochord actively expands in the nucleus pulposus by proliferation. Previous studies have looked at post-embryonic growth and proliferation and have found proliferation in the intervertebral discs until postnatal day 21,[24] but no embryonic studies exist.

Here we show that a marker of hypertrophy, Collagen 10, is expressed in the forming vertebrae after the notochord is already fully excluded from the vertebra. All elements of the spinal segment, including the developing vertebra, show little change in size or proliferation between E12.5 and E14.5, notably including the time period when the notochord begins segmentation. During segmentation, there is an increase in notochord cell proliferation seen only in the nucleus pulposus expansion of the notochord. It is only after the exclusion of the notochord is complete for many spinal levels that the vertebra dramatically expands (494%), through a process characterized by a large drop in density but not an increase in proliferation. Our data suggest that the encroachment by the vertebral cells does happen, but to a large extent this occurs after exclusion of the notochord is complete. Our work shows that, in addition to chondrogenic encroachment, notochord proliferation plays a critical role during segmentation.

2 | RESULTS

To establish a context for interrogating the cellular events of notochord segmentation, we first examined the process histologically in the developing mouse embryo. The intervertebral disc arises from two tissues: the mesenchyme from the sclerotome of the somite and the notochord. At E11.5, the notochord attracts sclerotome to migrate ventrally to surround the notochord.[25] At E12.5, there is a repeating density cell gradient within the sclerotome at every spinal level; with bands of higher density that give rise to the annulus fibrosus of the intervertebral disc, and bands of lower density that give rise to the vertebra (Figure 1). At 12.5, the notochord is a long thin cylinder of uniform diameter (20 μm) that stretches from the head to the tail of the embryo (Figure 1A). The ratio of the diameter of the notochord at the intervertebral disc to the diameter of the notochord at the vertebra is 1. However, by E14.5, the notochord is hourglass-shaped within each segmental unit, with the narrowest diameter at the vertebral body, and an expansion at the intervertebral disc (Figure 1B). The ratio of the diameter at the intervertebral disc compared to at the vertebra can gauge the

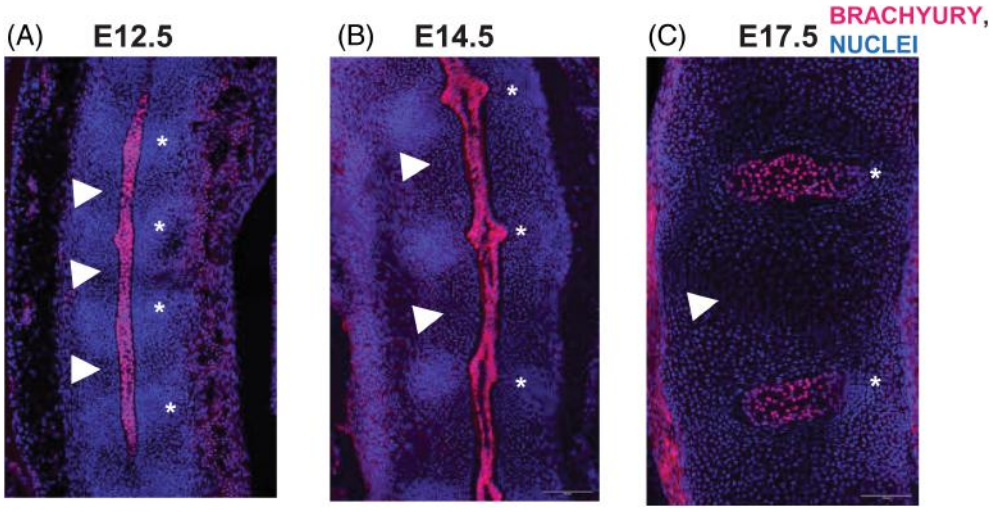

FIGURE 1 The Notochord is excluded from the vertebra progressively at embryonic day E14.5 though the vertebra undergo hypertrophy afterwords. (A) In the sagittal section at E12.5, the notochord, stained with Brachyury (magenta), is a narrow, cylindrical rod along the rostral caudal axis, and the annulus fibrosus of the intervertebral disc (*) is marked by higher cell density compared to the vertebra (arrowhead). (B) At E14.5, the notochord expands at the nucleus pulposus (*) and is gradually excluded from the vertebra (arrowhead). (C) At E17.5, notochord cells are completely excluded from the vertebra and reside exclusively in the nucleus pulposus of the intervertebral disc (*).

progression of the segmentation process with ranges from 2 to 10 at E14.5. A ratio of 2 indicates the notochord has expanded at the presumptive nucleus pulposus to double what is in the vertebra. At E17.5, the notochord is completely excluded from the vertebra and resides solely at the nucleus pulposus (Figure 1C).

In order to determine when vertebral cell hypertrophy occurs in relation to notochord exclusion, we leveraged the transgenic reporter Collagen10a1-mCherry[26] which is expressed in hypertrophic chondrocytes.[18,27,28] Across four embryos: (1) one spine did not express Col10mCh and had complete notochord exclusion in the thoracic and lumbar (Col10mCh was observed in the forelimb); (2) one had Col10mCh in cervical and thoracic levels but not in the lumbar which had complete notochord exclusion; (3) one had Col10mCh in thoracic levels and not in the distal tail which had complete notochord exclusion; and (4) one had Col10mCh in the palate but not the cervical spine which had complete notochord exclusion (Figure 2A). The Col10mCh expressing palate had a lower density than the cervical spine (Figure 2B). Furthermore, protein concentration visualized with Normalized Raman Imaging (NoRI) indicated minimal extracellular matrix deposition present in non-expressing cells, that is, 7th cervical vertebra, C7, compared to Col10mCh expressing hypertrophic chondrocytes at the palate (Figure 2C). 3D Cell volume measurements from NoRI acquisition further indicate that Col10mCh negative cells are not morphologically hypertrophic: cells expressing Col10mCh had a greater volume ($4750 \pm 1520\ \mu m^3$) than the cells not expressing Collagen 10mCh ($1680 \pm 383\ \mu m^3$; Figure 2D). The notochord is completely excluded from vertebra regardless of Collagen 10 expression.

We next examined the cell density of the axial tissues to observe changes relative to notochord exclusion from the vertebra. Local density is highest in the annulus fibrosus and lowest in the vertebra at E17.5 (Figure 3A). Within the mesenchyme surrounding the notochord, the regions forming vertebral bodies always have lower cell density than those forming the annulus fibrosus (Figure 3B). Notably, the cell density of both these mesenchymal tissues remained constant between E12.5 and E14.5. Subsequently however, the vertebral cell density decreased dramatically, by 56% to 0.0073 ± 0.0014 cells/μm^2 from E14.5 to E17.5, while the annulus fibrosus cell density decreased 46% to 0.015 ± 0.0036 cells/μm^2. In contrast, the notochord density dropped throughout this time period; from 0.020 ± 0.0035 cells/μm^2 at E12.2, to 0.012 ± 0.0037 cells/μm^2 at E14.5, and 0.0081 to ± 0.0027 cells/μm^2 at E17.5 (Figure 3C). The decrease in vertebral body cell density at the E17.5 is consistent with chondrogenic hypertrophic differentiation, that is, cell swelling and extracellular matrix deposition. Although the E12.5 and E14.5 mesenchymal densities are equivalent, the large range observed at E14.5 could support the prediction that the density decreases as the notochord narrows. Comparing the vertebral cell density at E14.5 against the notochord diameter ratio (Figure 3D) show that when the notochord diameter ratio is 2–4, the cell density is

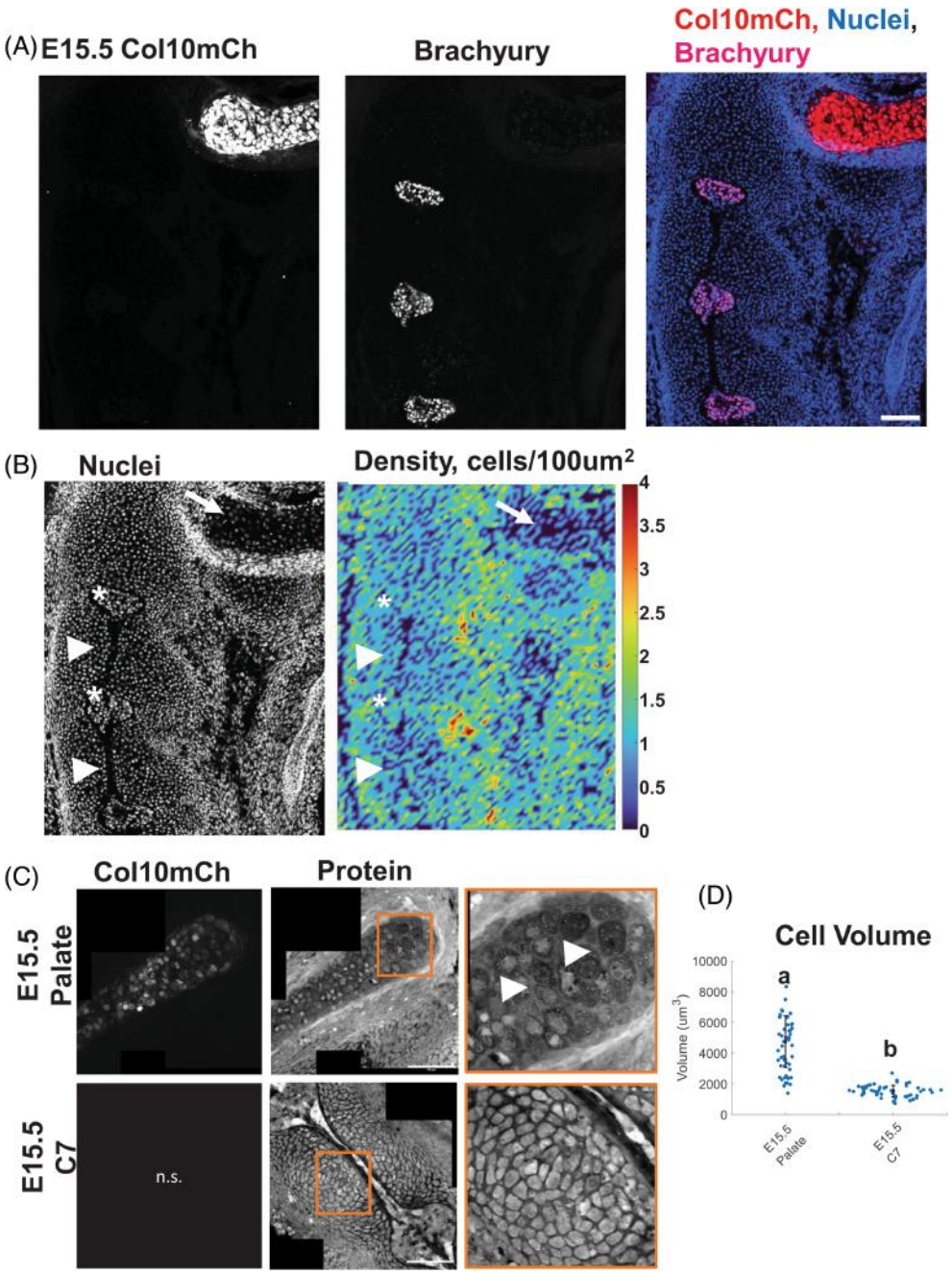

FIGURE 2 At E15.5, the notochord is excluded completely from both expressing and non-expressing Collagen 10 vertebra levels. (A) The palate, anterior to the cervical spine, has begun to express Collagen 10 (red). The cervical spine is not expressing Collagen 10 yet, but has completely excluded notochord with the totality solely residing in the nucleus pulposus. In three other spines (not shown), the level which expressed Collagen 10 was always anterior to the levels which have not expressed Collagen 10, and these posterior non-expressing vertebra had fully excluded the notochord. (B) The Collagen 10 expressing palate has a lower cell density (arrow) than the vertebra (arrowhead). (C) Comparison of Col10mCh expression and protein distribution in E15.5 palate and 7th cervical vertebra (C7) hypertrophic cartilage. Left column: Col10mCh fluorescence signal. The palate shows distinct Col10mCh-positive cells, while C7 shows no signal (n.s.). Middle column: Protein concentration visualized by Normalized Raman Imaging (NoRI). The palate exhibits a characteristic protein concentration profile in hypertrophic cartilage, with distinct cellular and extracellular matrix (ECM) regions. C7 shows a different protein distribution pattern. Right column: Enlarged areas (orange boxes) from the protein images. In the palate, arrowheads indicate regions of high protein concentration in the ECM surrounding hypertrophic chondrocytes. The C7 image shows a more uniform protein distribution across cells without the distinct ECM protein accumulation seen in the palate. (D) Comparison of cell volumes between E15.5 palate hypertrophic chondrocytes and E15.5 C7 chondrocytes. Col10mCh-positive E15.5 palate hypertrophic chondrocytes exhibit significantly larger cell volumes (4750 ± 1520 μm^3, median ± SD) than E15.5 C7 chondrocytes not expressing Col10mCh which show smaller cell volumes (1680 ± 383 μm^3, median ± SD). Each dot represents an individual cell measurement. Black bars indicate median ± SD for each group. Scale bars are 100 μm.

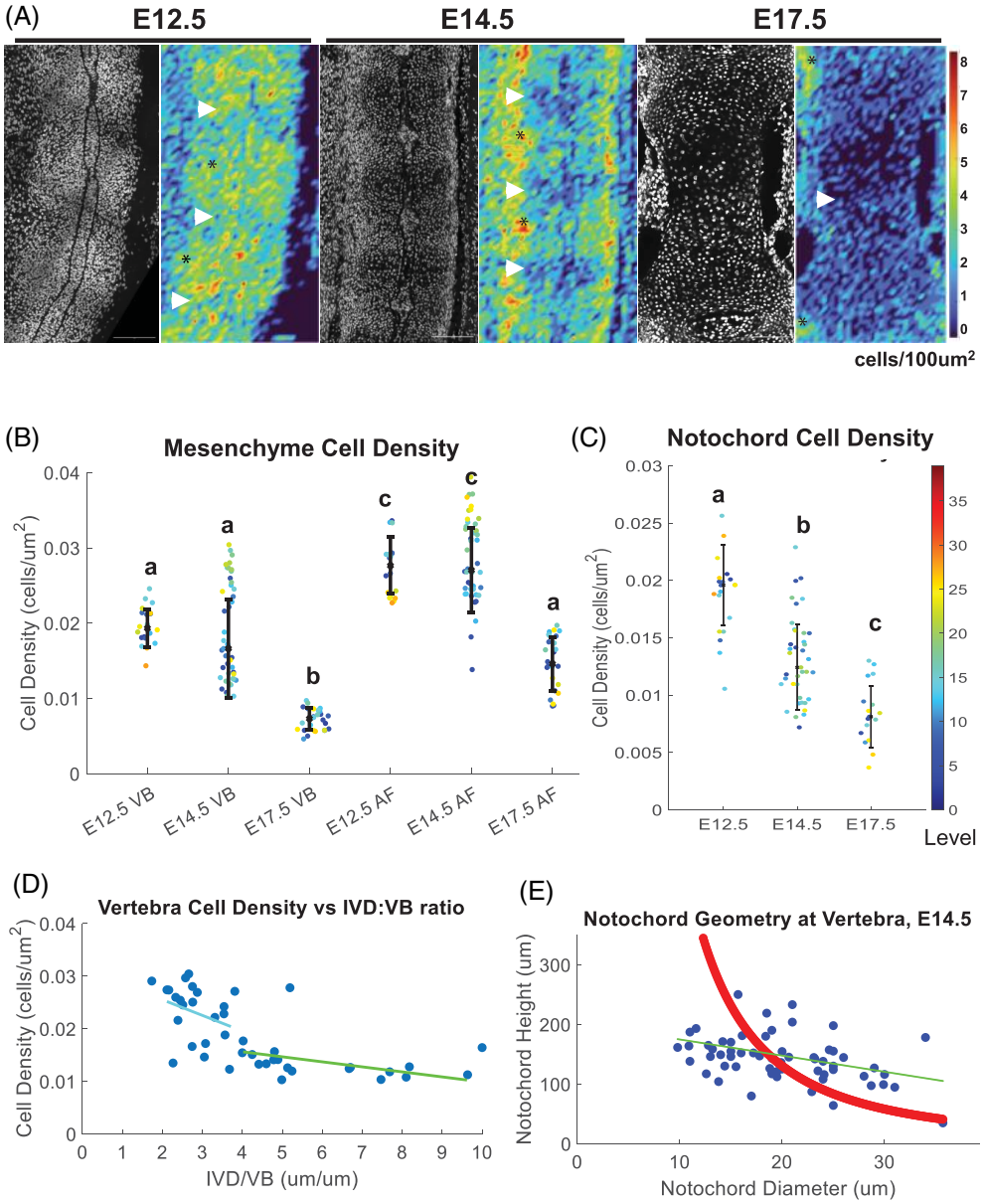

FIGURE 3 Vertebral cell density does not decrease until after the notochord is excluded at E17.5. (A) Representative density maps show localized peaks in the annulus fibrosus (*), and minima in the vertebra (arrowhead). (B) Within the mesenchyme, the vertebral body density is less than the annulus fibrosus at all timepoints, and both annulus fibrosus and vertebral body cell density drops at E17.5. (C) The notochord cell density decreased at every timepoint. Color bar indicates Spinal Level (Cervical 1–7, Thoracic 8–21, Lumbar 22–27). (D) At E14.5, the vertebral cell density for levels with notochord diameter ratio between 2 and 4 is 0.025 cells/μm^2, and decreases steadily at a rate of −0.0030 cells/μm^2/ratio ($R^2 = 0.08$). At ratios >4, the density drops 50% to 0.013 cells/μm^2 at a slower rate of −0.0010 cells/μm^2/ratio ($R^2 = 0.16$). (E) The decrease in notochord radius seen across the spine at E14.5 is not due to increased vertebral height. The observed height (blue) is linear (green, $y = -2.7x + 202$, $R^2 = 0.09$) and is does not follow to the expected increase in height if volume is conserved (red, $h = V/\text{pi}*r^2$ was solved $y = 1.1x^2 - 63x + 960$). Each point represents one spinal level from $n = 4$ embryos; bar and whiskers indicate median and standard deviation. Scale bars are 100 μm.

0.025 cells/μm^2, and decreases steadily at a rate of −0.0030 cells/μm^2/ratio (i.e., the density drops by about 10% per IVD/VB ratio increase of 1) ($R^2 = 0.08$). After the ratio increases from 4, the density drops 50% to 0.013 cells/μm^2 and decreases at a slower rate of −0.0010 cells/μm^2/ratio ($R^2 = 0.16$). The decreased vertebral cell density at E17.5 indicated that detectable vertebral cell density differences only arise after the notochord is mostly excluded, and the small drop in cell density at E14.5 alongside the drop in notochord diameter indicated that the decreased density could contribute to the earliest steps of notochord segmentation.

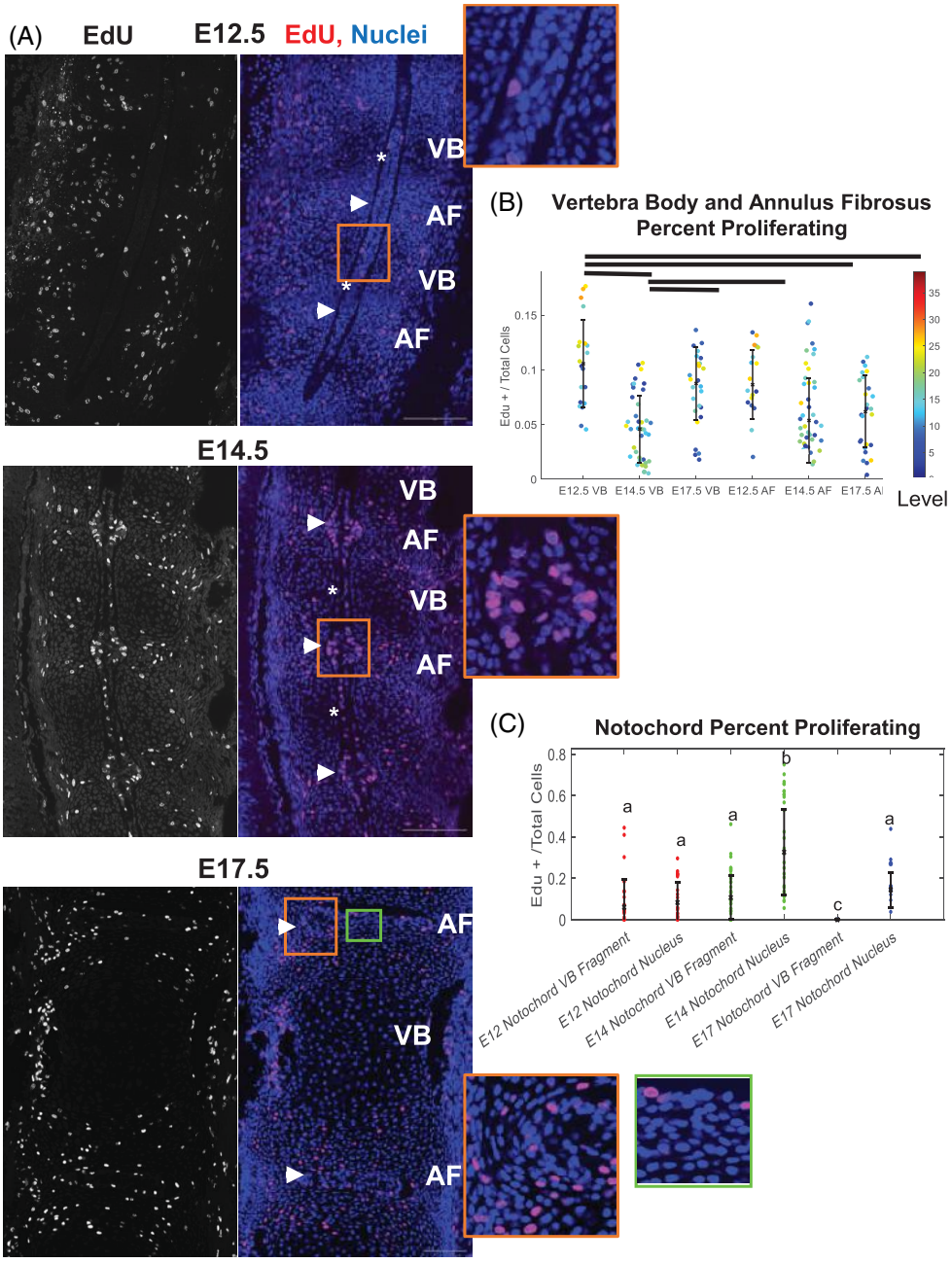

FIGURE 4 Proliferation is highest at the notochord expanding into the nucleus pulposus of the intervertebral disc. (A) Representative images from sagittal sections at E12.5, E14.5 and E17.5 have uniform proliferation except at the notochord at E14.5. Data are 60 min after EdU injection. (B) The vertebral body proliferation was 10% at E12.5, decreasing to 5% at E14.5 and rising again to 9% at E17.5. The annulus fibrosus proliferation did not vary and was 8%, 5% and 6% at E12.5, E14.5 and E17.5, respectively. (C) The notochord proliferation was 6% and 11% at the level of the vertebral fragment at E12.5 and E14.5, with no cells present at E17.5. In the notochord at the level of the intervertebral disc, 'Notochord Nucleus', proliferation was 9% at E12 and then increased significantly to 34% at E14 before dropping to 14% at E17. AF, annulus fibrosus of intervertebral disc; VB, vertebral body, * indicates Notochord VB fragment, arrowhead indicates Notochord Nucleus. Each point represents one spinal level from $n = 4$ embryos; bar and whiskers indicate median and standard deviation.

An alternative hypothesis is that the stretching of the vertebra through axial growth is responsible for narrowing of the notochord in the vertebral body fragment. Given the assumption that volume of the notochord fragment is conserved, the diameter would decrease exponentially as the height increases, as indicated by the solution for $h = V/\text{pi}*r^2$ with the median observed geometry at E14.5 (red line, Figure 3E). The actual height and diameter (blue) do not follow the expected relationship, and do not support the hypothesis.

Changes in density can occur through cell swelling, deposition of extracellular matrix or proliferation. To test the impact of this last parameter, we investigated proliferation in all the mesenchyme (the annulus fibrosus and the vertebra), and the notochord tissue which is split into the disappearing fragment at the level of the vertebra (Notochord VB Fragment) and the expanding notochord at the level of the intervertebral disc, that is, the nucleus pulposus (Notochord Nucleus) (Figure 4A). Our data show a slight reduction in proliferation after E12.5 across all tissue types except the portion of the notochord within the intervertebral expansion. The vertebral body percent proliferation varied across timepoints, it was 10% at E12.5, decreased to 5% at E14.5 and rose to 9% at E17.5. The annulus fibrosus proliferation did not vary with proliferation of

8%, 5% and 6% proliferation at E12.5, E14.5 and E17.5, respectively (Figure 4B). The proliferation at E12.5 were 6% in the notochord fragment at the level of the vertebra and 9% in the notochord at the level of the intervertebral disc, the nucleus pulposus expansion. The proliferation at E14.5 was 11% in the notochord fragment at the level of the vertebra, but increased to 34% in the notochord at the level of the intervertebral disc, the nucleus pulposus expansion. Proliferation strongly contributes to the expansion of the nucleus pulposus domain of the notochord. The proliferation at E17.5 was 14% in the notochord at the level of the intervertebral disc, the nucleus pulposus expansion, and the notochord fragment at the level of the vertebra is not present (Figure 4C).

In order to elucidate if the increased proliferation seen at E14.5 is sufficient to create the nucleus pulposus at E17.5, we ran logistic growth simulations using the observed proliferation, cell count, density and area. The logistic growth with rates equal to the observed proliferation at E12.5 for 5 days resulted in an estimated E17 notochord area of 8150 ± 3490 μm^2; the model using E14 proliferation for 3 days had an estimated area of 11,900 ± 3550 μm^2. The actual observed area at E17 was 53% greater than the model with E14 rates, and 108% greater than predicted with E12.5 cell number and proliferation (Figure 5A). The actual notochord area increased 21% between E12.5 and E14.5 and increased 177% between E14.5 and E17.5 (Figure 5B).

Taken together, our data support a model of embryonic spine formation where the initial segmentation of the notochord into discrete segments involves localized changes in proliferation, prior to hypertrophic swelling in the neighboring vertebral body regions. This is a dynamic process where the notochord and mesenchymal tissue that gives rise to the annulus fibrosus and vertebral bodies have a proliferation of 10% at E12.5, but by E14.5 the proliferation of the notochord at the intervertebral

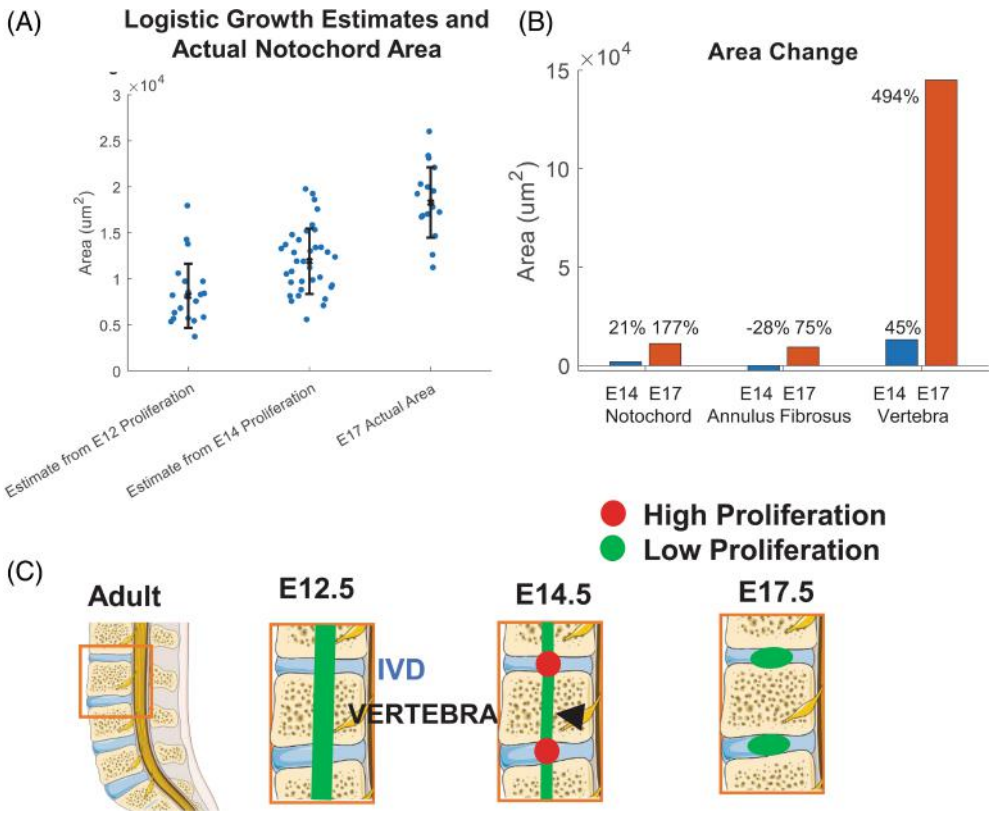

FIGURE 5 The proliferation increase at E14 is necessary to reach E17 Notochord size (A) Logistic models of observed proliferation at E12 and E14 show that the estimated notochord areas are 8150 and 11,900 μm^2 compared to the actual observed area at E17 of 18,300 μm^2. (B) The notochord area increased 21% from E12.5 to E14.5, whereas the annulus fibrosus area decreased by 28%; the vertebra area increased by 45%. The notochord area increased 177% from E14.5 to E17.5, and the annulus fibrosus increased 75% and the vertebra increased by 494%. (C) At E12.5, the vertebral has a lower density than the annulus fibrosus in the intervertebral disc (IVD), both have similar areas, and all tissues have 5%–10% proliferation. At E14.5, all areas increase slightly without a change in density, and the proliferation remains at around 10%, except notochord proliferation at the intervertebral expansion increases to 34% when it starts to expand into the nucleus pulposus (red). At E17.5, all areas increase substantially, densities drop most dramatically in the vertebra, and all proliferation is reduced. Each point represents one spinal level from $n = 4$ embryos; bar and whiskers indicate median and standard deviation.

expansion increases to 34%, while proliferation of the other tissues remains at 10%. At E17.5, density drops dramatically for the vertebral body portion of the mesenchyme, accompanied by an increase in area (Figure 5C).

3 | DISCUSSION

The current model in the field is that notochord is excluded from the vertebra as a result of chondrogenesis in the vertebra including deposition of proteoglycan-rich extracellular matrix or the hypertrophic swelling of the adjacent precursors of the vertebral bodies.[7,15,16] In the present study, we showed that hypertrophy (indicated by vertebra growth, Col10 expression and drop in cell density) occurs largely after the notochord is excluded from the vertebra, although there is reduction in cell density and early extracellular matrix deposition during exclusion. Starting shortly after exclusion begins, the notochord cells at the presumptive nucleus pulposus proliferate at a higher rate than before, and higher than in the vertebral fragment. Modeling results show that the increased notochord cell proliferation is necessary to approach the observed cell numbers present when the nucleus pulposus has fully formed. In chick, where the notochord is not excluded from the vertebra at hatching,[29] the vertebral cells undergo hypertrophy and express Collagen 10 mRNA starting at Stage 36 while the notochord remains in the vertebra,[28] instead of being restricted to the nucleus pulposus as in mouse and human. After the increase in proliferation, the nucleus pulposus increases in cross-sectional area, suggesting that proliferation underlies much of the intervertebral expansion, rather than being exclusively based on passive squeezing from the vertebral cells.

Together, these observations indicate that notochord exclusion occurs before hypertrophy and that proliferation plays a vital role in this process. In mice lacking the homeobox protein NKX3.2, the sclerotome largely fails to migrate around the ventral side of the notochord, but the notochord still produces swellings at the intervertebral disc,[23] supporting the hypothesis presented here that notochord cell autonomous processes impact nucleus pulposus formation. Signals driving the proliferative event, that is, the mechanism by which the nascent nucleus pulposus is expanded are not well understood. The notochordal cells could be responding cell autonomously or responding to external sources, as the notochord responds to the sclerotome (and vice versa) during segmentation of the chick spine.[25] There exists multiple reviews on known signaling pathways involved in spine formation and maintenance.[30–32] Brachyury, an auto-regulatory[33] T-box transcription factor associated with proliferation,[13,34,35] is critical for trunk and neural tube development.[33] Another candidate, the diffusible morphogen Sonic Hedgehog (SHH) which directs patterning of the ventral embryo,[36–38] is necessary for disc maintenance[39] and formation.[9] The feedback loop of Indian Hedgehog and parathyroid hormone-related protein is expressed in the healthy and degenerate intervertebral disc.[40] Other candidates include bone morphogenetic protein and Wnt signaling which are transcriptionally upregulated at E12.5 compared to P0.[41] Future studies could test the requirement of these candidates.

Our observation of dramatic growth at E17.5, is mirrored by postnatal observations of rapid growth, suggesting the embryonic growth observed here continues after birth. Postnatal growth of the IVD and vertebra can be described as logarithmic, plateauing at an average length of 600 μm and 2.5 mm by 9 weeks.[24] The number of mitotic cells expressing phospho-histone H3 reached a peak of 80 proliferating cells in both the nucleus pulposus and annulus fibrosus 1 week after birth, and declined to near zero at 4 weeks.[24] The notochord cells that relocate from the vertebral fragment could represent a proportion of the proliferating cells which could be tested with lineage tracing. At P1, the peripheral nucleus pulposus cells are more proliferative than the central cells and differentiate into the inner nucleus pulposus.[42]

Since cell density, measured here with nuclear staining, reflects both cell swelling and extracellular matrix deposition which occurs before hypertrophy, cell density alone cannot accurately assess chondrocyte hypertrophy. The average density could obfuscate local changes like cell condensation, but no evidence of this was observed in local density maps. The decrease in density at E14.5 as the notochord narrows indicates that there is atleast some expansion concurrent with notochord narrowing, perhaps from the transition from mesenchymal cells to chondrocytes proper, or potentially from proliferating chondrocytes to pre-hypertrophic chondrocytes. Consistent with the deposition of extracellular matrix before hypertrophy, vertebral precursor cells start to deposit glycosaminoglycans at E13.5, where chondrocyte hypertrophy coincides with nucleus pulposus overt development following, but neither before or during notochord squeezing.[17] Glycosaminoglycan deposition occurs before our observed cell density drop of 56% between E14.5 and E17.5, indicating that deposited extracellular matrix and initial stages of hypertrophy have begun by E14.5 and could be playing a role in notochord exclusion.

Nonetheless, average cell density did not change between E12.5 and E14.5, indicating that vertebral cell hypertrophy is in the early stage when the notochord is changing into distinct nucleus pulposus. This article used the expression of Collagen 10 as a marker of hypertrophic

chondrocytes.[18,28,43] Testing whether endochondral ossification is necessary to complete the exclusion of the notochord from the vertebra would require observing the notochord in embryos without hypertrophy, perhaps by knocking out a required hypertrophic factor such as the DNA binding protein Runx2.[44–46] The relationship between nucleus pulposus loading and annulus fibrosus structure is that there is energy stored in the annulus fibrosus from nucleus pulposus pressurization.[47] The nucleus pulposus is pressurized under compressive loading, which exerts tension on the annulus fibrosus, also known as hoop stress,[48,49] and the annulus fibrosus is anisotropic, having greater tensile modulus than compressive and shear modulus.[50] Future studies may test the hypothesis that expansion of the nucleus pulposus differentiates the annulus fibrosus[51–53] and if proliferation is necessary for the notochord to nucleus pulposus transition.

Our data show that although vertebra hypertrophy does occur, the onset is after notochord segmentation has completed, and the bulk of growth occurs after segmentation is complete. The vertebral growth is driven by either cell swelling or extracellular matrix deposition, as indicated by stable proliferation and drop in cell density. The notochord volume is increasing at E14.5, amidst segmentation, driven by an increase in proliferation which is higher in the intervertebral expansion into nucleus pulposus. Together, our data support a model of notochord segmentation that proliferation of notochord cells expands the nucleus pulposus before hypertrophy of the vertebra.

4 | EXPERIMENTAL PROCEDURES

Collagen 10 Expression: Collagen10a1-mCherry fluorescent protein reporter[26] embryos were collected at embryonic day 15.5, fixed overnight in 4% paraformaldehyde (Fischer Scientific, AA47377), equilibrated in 1:1 30% sucrose and Optimum Cutting Temperature media (VWR, 25608–930), sectioned at 14um, and stained with brachyury (1:200, RND Systems, AF2085) overnight at 4° followed by secondary incubation (1:400, Jackson Immuno Research Laboratories Inc., 705–545-003) counterstained with 4′,6-Diamidino-2-Phenylindole, Dihydrochloride, Dapi (Thermo-Fischer, D1306).

Proliferation: Timed pregnant dams (Jackson Labs, 000664) were injected with 100 mg/kg thymidine analogue 5-Ethynyl-2′-deoxyuridine (EdU) (Thermo-Fischer, A10044) 60 min before embryo collection at E12.5, E14.5 and E17.5. The 60 min window is the time for maximum incorporation in embryonic tissue.[54] After fixation, embryos were equilibrated as above, sectioned at 16um and stained using the EdU Click-It Imaging Kit (Invitrogen, C10339) followed by brachyury (1:200, RND Systems, AF2085) and a nuclear counter stain, Draq5 (Abcam, AB108410). All animal procedures were approved by the Institutional Animal Care and Use Committee at Harvard Medical School.

All images except NoRI images were collected with a 40× objective on an Nikon Eclipse Ti2 (MVI, Avon, MA) microscope equipped with a confocal spinning disc scanner Yokogawa CSU-W1 and an Andor Zyla sCMOS detector. Schematics use art from Servier Medical Art (licensed CC BY 4.0).

Image Analysis: Nuclei were segmented using StarDist trained with dsb2018_heavy_augment model[55,56] within the opensource QuPath software.[57] Nuclei $<3\ \mu m^2$ were discarded. The cell density was calculated by counting the nuclei and dividing by the area. For density maps, a custom Matlab script (Natick, MA) imported the spatial coordinates of the nuclei centra and calculated the density in 100 sq. micron bins. To separate the annulus fibrosus and vertebra, the cell density and nuclear stain intensity were used, where the regions of lowest density and lowest minimum nuclear dye intensity marked the vertebra. Proliferating cells were identified based on the mean EdU intensity within the segmented nucleus. A single spinal level is made up of a vertebra (for example cervical level 6) with the superior intervertebral disc (C5-C6), and enclosed notochord. The notochord was identified by staining with an antibody against the well-established molecular marker, brachyury.

The diameter at the intervertebral expansion compared to the diameter at the vertebra is used to measure the progression of notochord exclusion with a ratio of 2 meaning the diameter in the disc is twice what it is in the vertebra. Statistics were done using Kruskal-Wallis test which is a nonparametric ANOVA, and bars and letters indicate statistically different groups at $p < 0.05$. Each dot is the measurement of one level, multiple levels were measured per embryo. There were four embryos from two litters at each timepoint.

Mathematical Model: The cell proliferation model uses logistic growth ($dN/dt = r[K-N/K]*N$) which is exponential growth with the following parameters: a total growth limitation called the carrying capacity (K)[58] which is set to three times the observed E17 cell number as an estimate of the maximum cell population given restricted space and nutrition and anabolic factors; growth rate (r) equal to the observed proliferation at E14.5 and E12.5; and initial population size (N) equal to the observed cell number. The modeled population was calculated for each observed proliferation and cell number at each timepoint and the E12.5 and E14.5 model

were modeled for 5 and 3 days, respectively. The model was written in Matlab (Mathworks, Natick, MA).

Normalized Raman Imaging (NoRI): NoRI was performed as previously described.[59] Briefly, given the objective of illustrating the volumetric profile between hypertrophic chondrocytes at palate and the cervical vertebra chondrocytes, and ensuring consistency across the process, a single Col10mCh embryo was collected at embryonic day 15.5. The embryo was fixed overnight in 4% formaldehyde (Fischer Scientific, AA47377), equilibrated in Phosphate Buffered Saline (PBS, Invitrogen, AM9625), embedded overnight in 0.36% gelatin, 22.5% albumin, and 5% formaldehyde in 1X PBS, then sectioned sagittally into 100 μm thick slices using a Leica vibratome (Leica, VT 1000 M) to preserve the 3D volume and morphology of vertebra cells. The slices were stained overnight with DAPI (1 μg/mL, Thermo-Fisher, D1306) at room temperature, and re-equilibrated in PBS. Slices were mounted onto a thin chambered slide with 120 μm spacers (Grace Bio-Labs, 654,006) in PBS to maintain their thickness. The mounted samples were then subjected to NoRI microscopy and confocal fluorescence microscopy to detect mCherry signal. Slices that encompass palate hypertrophic chondrocytes and cervical vertebra were selected for analysis. NoRI measures the absolute protein and lipid concentration of a tissue in situ, in 3D, and the cell boundaries can be readily determined by the sharp differences in protein concentration as well as lipid concentration. 3D cell boundaries were manually delineated for every 2–3 z-stack slices, with interpolation for the intervening slices, yielding 3D segmentations of cells of interest. Cell volumes were calculated by measuring the voxel counts of the segmentations and multiplying by the pixel dimensions (unit voxel = 0.41432 × 0.41432 × 1 μm). All image drawing and analysis were performed with a custom script in ImageJ (National Institute of Health).

FUNDING INFORMATION

Grant sponsor: NIAMS—Grant number: F32AR076226.

ORCID

Rose G. Long https://orcid.org/0000-0001-9999-9288
Clifford J. Tabin https://orcid.org/0000-0002-2957-4871

REFERENCES

1. Christ B, Ordahl CP. Early stages of chick somite development. *Anat Embryol (Berl)*. 1995;191(5):381-396. doi:10.1007/BF00304424
2. Krull CE, Lansford R, Gale NW, et al. Interactions of Eph-related receptors and ligands confer rostrocaudal pattern to trunk neural crest migration. *Curr Biol*. 1997;7(8):571-580. doi:10.1016/S0960-9822(06)00256-9
3. Ward L, Evans SE, Stern CD. A resegmentation-shift model for vertebral patterning. *J Anat*. 2017;230(2):290-296. doi:10.1111/joa.12540
4. Bagnall KM, Higgins SJ, Sanders EJ. The contribution made by a single somite to the vertebral column: experimental evidence in support of resegmentation using the chick–quail chimaera model. *Development*. 1988;103(1):69-85. doi:10.1242/dev.103.1.69
5. Aoyama H, Asamoto K. The developmental fate of the rostral/caudal half of a somite for vertebra and rib formation: experimental con®rmation of the resegmentation theory using chick-quail chimeras. *Mech Dev*. 2000;99(1-2):71-82.
6. Choi K, Cohn MJ, Harfe BD. Identification of nucleus pulposus precursor cells and notochordal remnants in the mouse: Implications for disk degeneration and chordoma formation. *Dev Dyn*. 2008;237(12):3953-3958. doi:10.1002/dvdy.21805
7. McCann M, Séguin C. Notochord cells in intervertebral disc development and degeneration. *J Dev Biol*. 2016;4(1):3. doi:10.3390/jdb4010003
8. Dahia CL, Mahoney E, Wylie C. Shh signaling from the nucleus pulposus is required for the postnatal growth and differentiation of the mouse intervertebral disc. *PLoS One*. 2012;7(4):e35944. doi:10.1371/journal.pone.0035944
9. Choi KS, Lee C, Harfe BD. Sonic hedgehog in the notochord is sufficient for patterning of the intervertebral discs. *Mech Dev*. 2012;129(9–12):255-262. doi:10.1016/j.mod.2012.07.003
10. Ghaith AK, Akinduro OO, Perez-Vega C, et al. Association between immunohistochemical markers and tumor progression following resection of spinal chordomas: a multicenter study. *J Neurosurg Spine*. 2023;39(5):1-9. doi:10.3171/2023.6.SPINE23348
11. Pandiar D, Thammaiah S. Physaliphorous cells. *J Oral Maxillofac Pathol*. 2018;22(3):296. doi:10.4103/jomfp.JOMFP_265_18
12. Manzone P, Fiore N, Forlino D, Alcala M, Cabrera CF. Chordoma of the lumbar L2 vertebra: case report and review of the literature. *Eur Spine J*. 1998;7(3):252-256. doi:10.1007/s005860050068
13. Yang XR, Ng D, Alcorta DA, et al. T (brachyury) gene duplication confers major susceptibility to familial chordoma. *Nat Genet*. 2009;41(11):1176-1178. doi:10.1038/ng.454
14. Bai J, Shi J, Li C, et al. Whole genome sequencing of skull-base chordoma reveals genomic alterations associated with recurrence and chordoma-specific survival. *Nat Commun*. 2021;12(1):757. doi:10.1038/s41467-021-21026-5
15. Smith LJ, Nerurkar NL, Choi KS, Harfe BD, Elliott DM. Degeneration and regeneration of the intervertebral disc: lessons from development. *Dis Model Mech*. 2011;4(1):31-41. doi:10.1242/dmm.006403
16. Aszódi A, Chan D, Hunziker E, Bateman JF, Fässler R. Collagen II is essential for the removal of the notochord and the formation of intervertebral discs. *J Cell Biol*. 1998;143(5):1399-1412. doi:10.1083/jcb.143.5.1399
17. Smits P, Lefebvre V. Sox5 and Sox6 are required for notochord extracellular matrix sheath formation, notochord cell survival and development of the nucleus pulposus of intervertebral discs. *Development*. 2003;130(6):1135-1148. doi:10.1242/dev.00331
18. de Frutos CA, Vega S, Manzanares M, et al. Snail1 is a transcriptional effector of fgfr3 signaling during chondrogenesis

and achondroplasias. *Dev Cell*. 2007;13(6):872-883. doi:10.1016/j.devcel.2007.09.016
19. Smits P, Li P, Mandel J, et al. The transcription factors L-Sox5 and Sox6 are essential for cartilage formation. *Dev Cell*. 2001;1(2):277-290.
20. Yamashita S, Miyaki S, Kato Y, et al. L-Sox5 and Sox6 proteins enhance chondrogenic miR-140 MicroRNA expression by strengthening dimeric Sox9 activity. *J Biol Chem*. 2012;287(26):22206-22215. doi:10.1074/jbc.M112.343194
21. de Crombrugghe B, Lefebvre V. Toward understanding SOX9 function in chondrocyte differentiation.
22. Paavola LG, Wilson DB, Center EM. Histochemistry of the developing notochord, perichordal sheath and vertebrae in Danforth's short-tail (Sd) and normal C57BL/6 mice. *Development*. 1980;55(1):227-245. doi:10.1242/dev.55.1.227
23. Lettice LA, Purdie LA, Carlson GJ, Kilanowski F, Dorin J, Hill RE. The mouse bagpipe gene controls development of axial skeleton, skull, and spleen. *Proc Natl Acad Sci*. 1999;96(17):9695-9700. doi:10.1073/pnas.96.17.9695
24. Dahia CL, Mahoney EJ, Durrani AA, Wylie C. Postnatal Growth, Differentiation, and Aging of the Mouse Intervertebral Disc. *Spine*. 2009;34(5):447-455. doi:10.1097/BRS.0b013e3181990c64
25. Ward L, Pang ASW, Evans SE, Stern CD. The role of the notochord in amniote vertebral column segmentation. *Dev Biol*. 2018;439(1):3-18. doi:10.1016/j.ydbio.2018.04.005
26. Maye P, Fu Y, Butler DL, et al. Generation and characterization of Col10a1 -mcherry reporter mice. *Genesis*. 2011;49(5):410-418. doi:10.1002/dvg.20733
27. Castagnola P, Dozin B, Moro G, Cancedda R. Changes in the expression of collagen genes show two stages in chondrocyte differentiation in vitro. *J Cell Biol*. 1988;106(2):461-467. doi:10.1083/jcb.106.2.461
28. Iyama K, Ninomiya Y, Olsen BR, Linsenmayer TF, Trelstad RL, Hayashi M. Spatiotemporal pattern of type X collagen gene expression and collagen deposition in embryonic chick vertebrae undergoing endochondral ossification. *Anat Rec*. 1991;229(4):462-472. doi:10.1002/ar.1092290405
29. Ghazanfari S, Werner A, Ghazanfari S, Weaver JC, Smit TH. Morphogenesis of aligned collagen fibers in the annulus fibrosus: Mammals versus avians. *Biochem Biophys Res Commun*. 2018;503(2):1168-1173. doi:10.1016/j.bbrc.2018.06.136
30. Alkhatib B, Ban GI, Williams S, Serra R. IVD development: nucleus pulposus development and sclerotome specification. *Curr Mol Biol Rep*. 2018;4(3):132-141. doi:10.1007/s40610-018-0100-3
31. Williams S, Alkhatib B, Serra R. Development of the axial skeleton and intervertebral disc. *Elsevier: Current Topics in Developmental Biology*. Vol 133. Elsevier; 2019:49-90. doi:10.1016/bs.ctdb.2018.11.018
32. Mohanty S, Dahia CL. Defects in intervertebral disc and spine during development, degeneration, and pain: New research directions for disc regeneration and therapy. *WIREs Dev Biol*. 2019;8(4):e343. doi:10.1002/wdev.343
33. Kemmler CL, Smolikova J, Moran HR, et al. Conserved enhancers control notochord expression of vertebrate Brachyury. *Nat Commun*. 2023;14(1):6594. doi:10.1038/s41467-023-42151-3
34. Postma AV, Alders M, Sylva M, et al. Mutations in the T (brachyury) gene cause a novel syndrome consisting of sacral agenesis, abnormal ossification of the vertebral bodies and a persistent notochordal canal. *J Med Genet*. 2014;51(2):90-97. doi:10.1136/jmedgenet-2013-102001
35. Zhu J, Kwan KM, Mackem S. Putative oncogene Brachyury (T) is essential to specify cell fate but dispensable for notochord progenitor proliferation and EMT. *Proc Natl Acad Sci*. 2016;113(14):3820-3825. doi:10.1073/pnas.1601252113
36. Johnson RL, Laufer E, Riddle RD, Tabin C. Ectopic expression of Sonic hedgehog alters dorsal-ventral patterning of somites. *Cell*. 1994;79(7):1165-1173. doi:10.1016/0092-8674(94)90008-6
37. Fan CM, Tessier-Lavigne M. Patterning of mammalian somites by surface ectoderm and notochord: Evidence for sclerotome induction by a hedgehog homolog. *Cell*. 1994;79(7):1175-1186. doi:10.1016/0092-8674(94)90009-4
38. Chamberlain CE, Jeong J, Guo C, Allen BL, McMahon AP. Notochord-derived Shh concentrates in close association with the apically positioned basal body in neural target cells and forms a dynamic gradient during neural patterning. *Development*. 2008;135(6):1097-1106. doi:10.1242/dev.013086
39. Bonavita R, Vincent K, Pinelli R, Dahia CL. Formation of the sacrum requires down-regulation of sonic hedgehog signaling in the sacral intervertebral discs. *Biol Open*. 2018;7(7):bio.035592. doi:10.1242/bio.035592
40. Bach FC, de Rooij KM, Riemers FM, et al. Hedgehog proteins and parathyroid hormone-related protein are involved in intervertebral disc maturation, degeneration, and calcification. *JOR Spine*. 2019;2(4):e1071. doi:10.1002/jsp2.1071
41. Peck SH, McKee KK, Tobias JW, Malhotra NR, Harfe BD, Smith LJ. Whole Transcriptome Analysis of Notochord-Derived Cells during Embryonic Formation of the Nucleus Pulposus. *Sci Rep*. 2017;7(1):10504. doi:10.1038/s41598-017-10692-5
42. Tan Z, Chen P, Dong X, et al. Progenitor-like cells contributing to cellular heterogeneity in the nucleus pulposus are lost in intervertebral disc degeneration. *Cell Rep*. 2024;43(6):114342. doi:10.1016/j.celrep.2024.114342
43. Kozhemyakina E, Lassar AB, Zelzer E. A pathway to bone: signaling molecules and transcription factors involved in chondrocyte development and maturation. *Development*. 2015;142(5):817-831. doi:10.1242/dev.105536
44. Xiao ZS, Liu S, Hinson TK, Quarles LD. Characterization of the upstream mouse Cbfa1/Runx2 promoter*. *J Cell Biochem*. 2001;82(4):647-659. doi:10.1002/jcb.1192
45. Inada, M, YasuI, T, Endo, N, Komori, T. Maturational disturbance of chondrocytes in Cbfa1-deficient mice. 1999.
46. Fujita T, Azuma Y, Fukuyama R, et al. Runx2 induces osteoblast and chondrocyte differentiation and enhances their migration by coupling with PI3K-Akt signaling. *J Cell Biol*. 2004;166(1):85-95. doi:10.1083/jcb.200401138
47. Michalek AJ, Gardner-Morse MG, Iatridis JC. Large residual strains are present in the intervertebral disc annulus fibrosus in the unloaded state. *J Biomech*. 2012;45(7):1227-1231. doi:10.1016/j.jbiomech.2012.01.042
48. Bowles RD, Setton LA. Biomaterials for intervertebral disc regeneration and repair. *Biomaterials*. 2017;129:54-67. doi:10.1016/j.biomaterials.2017.03.013

49. Sivakamasundari V, Lufkin T. Bridging the Gap: understanding embryonic intervertebral disc development. *Cell Dev Biol*. 2012; 1(2):103.
50. Long RG, Torre OM, Hom WW, Assael DJ, Iatridis JC. Design requirements for annulus fibrosus repair: review of forces, displacements, and material properties of the intervertebral disk and a summary of candidate hydrogels for repair. *J Biomech Eng*. 2016;138(2):021007. doi:10.1115/1.4032353
51. Beckett M, Ralphs JR, Caterson B, Hayes AJ. The transmembrane heparan sulphate proteoglycan syndecan-4 is involved in establishment of the lamellar structure of the annulus fibrosus of the intervertebral disc. *Eur Cell Mater*. 2015;30:69-88. doi:10.22203/eCM.v030a06
52. Canty EG, Starborg T, Lu Y, et al. Actin Filaments Are Required for Fibripositor-mediated Collagen Fibril Alignment in Tendon. *J Biol Chem*. 2006;281(50):38592-38598. doi:10.1074/jbc.M607581200
53. Hayes AJ, Benjamin M, Ralphs JR. Role of actin stress fibres in the development of the intervertebral disc: Cytoskeletal control of extracellular matrix assembly. *Dev Dyn*. 1999;215(3):179-189.
54. Packard DS, Menzies RA, Skalko RG. Incorporation of thymidine and its analogue, bromodeoxyuridine, into embryos and maternal tissues of the mouse. *Differentiation*. 1973;1(6):397-405. doi:10.1111/j.1432-0436.1973.tb00137.x
55. Weigert M, Schmidt U, Haase R, Sugawara K, Myers G. Star-convex polyhedra for 3D object detection and segmentation in microscopy. *2020 IEEE Winter Conference on Applications of Computer Vision (WACV)*. IEEE; 2020:3655-3662. doi:10.1109/WACV45572.2020.9093435
56. Schmidt U, Weigert M, Broaddus C, Myers G. Cell detection with star-convex polygons. 11071:2018, 265-2273. doi:10.1007/978-3-030-00934-2_30
57. Bankhead P, Loughrey MB, Fernández JA, et al. QuPath: Open source software for digital pathology image analysis. *Sci Rep*. 2017;7(1):16878. doi:10.1038/s41598-017-17204-5
58. Kilian HG, Bartkowiak D, Kaufmann D, Kemkemer R. The General Growth Logistics of Cell Populations. *Cell Biochem Biophys*. 2008;51(2–3):51-66. doi:10.1007/s12013-008-9012-9
59. Oh S, Lee C, Yang W, et al. Protein and lipid mass concentration measurement in tissues by stimulated Raman scattering microscopy. *Proc Natl Acad Sci*. 2022;119(17):e2117938119. doi:10.1073/pnas.2117938119

How to cite this article: Long RG, Lee C, Tabin CJ. Active cell proliferation contributes to the enlargement of the nascent nucleus pulposus. *Developmental Dynamics*. 2025;1-12. doi:10.1002/dvdy.70005